# Supporting Information: Spatially resolved modelling of $NH_3$ cracking in warm plasma

Rubén Quiroz Marnef*[1], Stein Maerivoet*[1,2], Ivan Tsonev[1], Francois Reniers[2] and Annemie Bogaerts[1]

[1] Research group PLASMANT, Department of Chemistry, University of Antwerp, Universiteitsplein 1, BE-2610 Wilrijk-Antwerp, Belgium
[2] Chemistry of Surfaces, Interfaces and Nanomaterials, Faculty of Sciences, Université Libre de Bruxelles, CP255, Avenue F.D. Roosevelt 50, B-1050 Brussels, Belgium

* These authors contributed equally to the work

E-mail: ruben.quirozmarnef@uantwerpen.be; stein.maerivoet@uantwerpen.be; annemie.bogaerts@uantwerpen.be

## S.1. All boundary conditions of the 2D model

Figure S1 presents the entire geometry of the pin-to-pin reactor, like Figure 3 of the main paper, but with the numbers of the boundaries indicated, to help the reader understand Table S1.

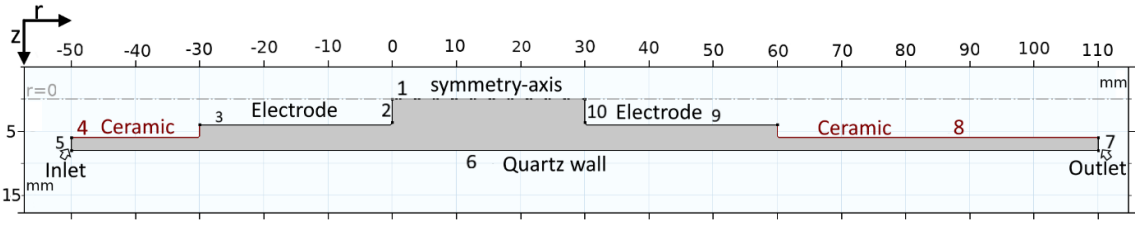


Figure S1 Geometry with boundaries numbered.

Table S1 Overview of all boundary conditions in the 2D model (see numbers of the boundaries in Figure S1). $\Delta H$ is the sensible enthalpy (kJ/mol), $\sigma_{SB}$ is the Stefan-Boltzmann constant (W/(m$^2$ K$^4$)), $T_{ext}$ is the external temperature (293.15 K), $\epsilon$ is the emissivity of quartz (dimensionless).

| Boundary | Heat transfer | Electrical Currents | Gas flow | Chemistry |
|---|---|---|---|---|
| **1** | Axial symmetry | Axial symmetry | $v_r = 0$<br>$v_\phi = 0$ | Axial symmetry |
| **2** | Thermal insulation<br>$\vec{n} \cdot \vec{q} = 0$ | Terminal<br>$\int_{\partial\Omega} \vec{J} \cdot \vec{n}\, dS = I_0$<br>The integral runs over boundary 2 and 3 | No slip wall<br>$\vec{v} = 0$ | No flux<br>$-\vec{n} \cdot \vec{J_i} = 0$ |

| | | | | |
|---|---|---|---|---|
| **3** | Heat flux<br>$-\vec{n} \cdot \vec{q} = q_0$<br>$q_0 = h\Delta T$<br>$h = 20\frac{W}{Km^2}$ | Terminal<br>$\int_{\partial\Omega} \vec{J} \cdot \vec{n}\, dS = I_0$<br>The integral runs over boundary 2 and 3 | No slip wall<br>$\vec{v} = 0$ | No flux<br>$-\vec{n} \cdot \vec{J_i} = 0$ |
| **4,8** | Thermal insulation<br>$\vec{n} \cdot \vec{q} = 0$ | Electrical Insulation<br>$\vec{n} \cdot \vec{J} = 0$ | No slip wall<br>$\vec{v} = 0$ | No flux<br>$-\vec{n} \cdot \vec{J_i} = 0$ |
| **5** | Inflow<br>$-\vec{n} \cdot \vec{q} = \rho\Delta H\, \vec{v} \cdot \vec{n}$<br>$\Delta H = \int_{T_{ext}}^{T} C_p dT$ | Electrical Insulation<br>$\vec{n} \cdot \vec{J} = 0$ | Inlet<br>$v_r = v_{r_0}$<br>$v_\phi = v_{\phi_0}$<br>$v_z = v_{z_0}$ | Inflow<br>$\omega_i = \omega_{i_0}$ |
| **6** | Heat flux<br>$-\vec{n} \cdot \vec{q} = q_0$<br>$q_0 = h\Delta T$<br>$+\epsilon\sigma_{SB}(T_{ext}^4 - T^4)$<br>h for external natural convection[1,2]<br>$\epsilon = 0.75$[3] | Electrical Insulation<br>$\vec{n} \cdot \vec{J} = 0$ | No slip wall<br>$\vec{v} = 0$ | No flux<br>$-\vec{n} \cdot \vec{J_i} = 0$ |
| **7** | Thermal insulation<br>$\vec{n} \cdot \vec{q} = 0$ | Electrical Insulation<br>$\vec{n} \cdot \vec{J} = 0$ | Outlet<br>$[-p\boldsymbol{I} + \boldsymbol{K}]\, \vec{n} = 0$ | No diffusion-flux<br>$-\vec{n} \cdot \rho D_i^m \vec{\nabla}\omega_i = 0$ |
| **9** | Heat flux<br>$-\vec{n} \cdot \vec{q} = q_0$<br>$q_0 = h\Delta T$<br>$h = 20\frac{W}{Km^2}$ | Ground<br>$V = 0$ | No slip wall<br>$\vec{v} = 0$ | No flux<br>$-\vec{n} \cdot \vec{J_i} = 0$ |
| **10** | Thermal insulation<br>$\vec{n} \cdot \vec{q} = 0$ | Ground<br>$V = 0$ | No slip wall<br>$\vec{v} = 0$ | No flux<br>$-\vec{n} \cdot \vec{J_i} = 0$ |

## S.2. Thermodynamic equilibrium data

The thermodynamic equilibrium of a thermal system, which is just dependent on $T_g$, will at high enough gas temperatures, yield electrons from associative ionization. This is complemented with an electron density, which is used to calculate the electrical conductivity of an equilibrated system. While the real conductivity in the plasma system, which is subject to an external electric field, will be different, we use the equilibrium electrical conductivity in the 2D axisymmetric model, as we do not have the computational power to solve the electron energy balance combined with all other physics included in the model. Naidis et al[4] reported that the differences between non-LTE-calculated and LTE-calculated conductivities were small at high currents (>50 mA). As expected, the Joule heating heat source shape will differ depending on the electrical conductivity of the system. However, section S.7. in this SI presents an analysis of the effect of the heat source shape on the main plasma metrics, from which we see that some deviation of the heat source shape, and thus of the electrical conductivity, will not influence the plasma metrics, as long as the total deposited energy is equal.

Figure S2 shows the temperature-dependent electrical conductivity used to calculate the electrical current and heat deposited (see section 2.4 in the main paper). The electrical current is extremely low for temperatures below 1500 K as there are almost no electrons below this temperature. The conductivity increases exponentially with temperature, as expected.

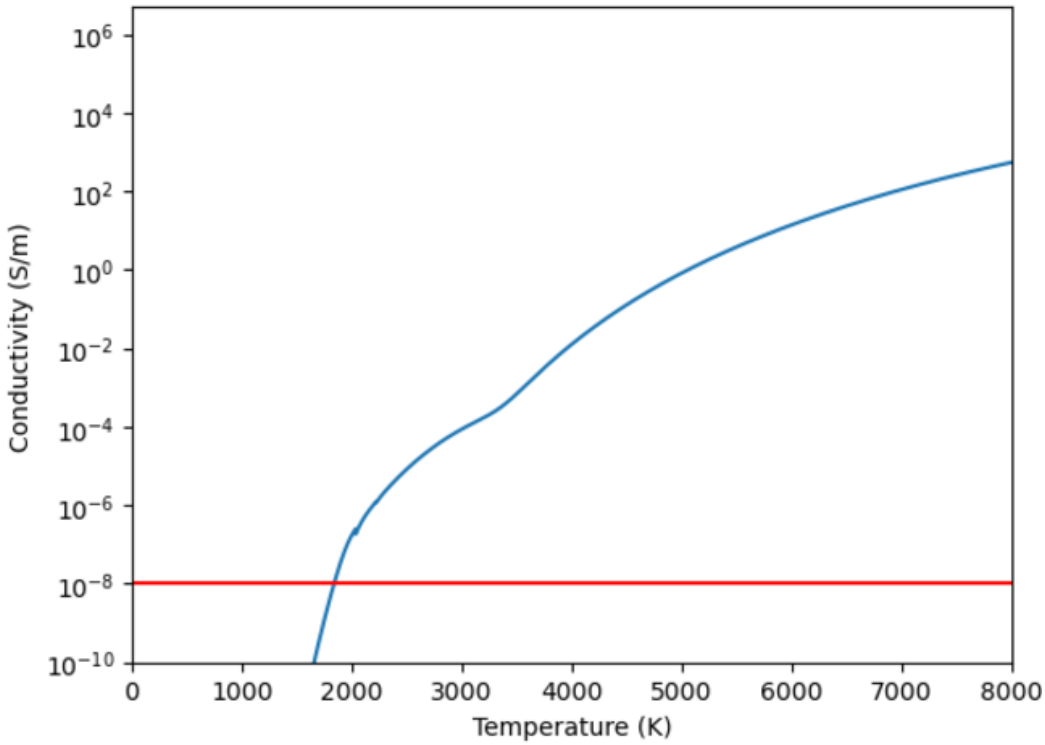


Figure S2. Electrical conductivity for $NH_3$ at thermal equilibrium, as a function of temperature. The red line is the lower bound used for numerical stability.

Figure S3 presents the molar fractions at thermodynamics equilibrium, as a function of temperature, both on a linear scale (a) and on a logarithmic scale (b). We can see that $NH_3$ is unstable at elevated temperatures, while the ionization degree is quite low over the full

temperature range (maximum $2.2 \times 10^{-3}$ at 8000 K). This information is used to calculate the conductivity, as mentioned in section 2.4 of the main paper.

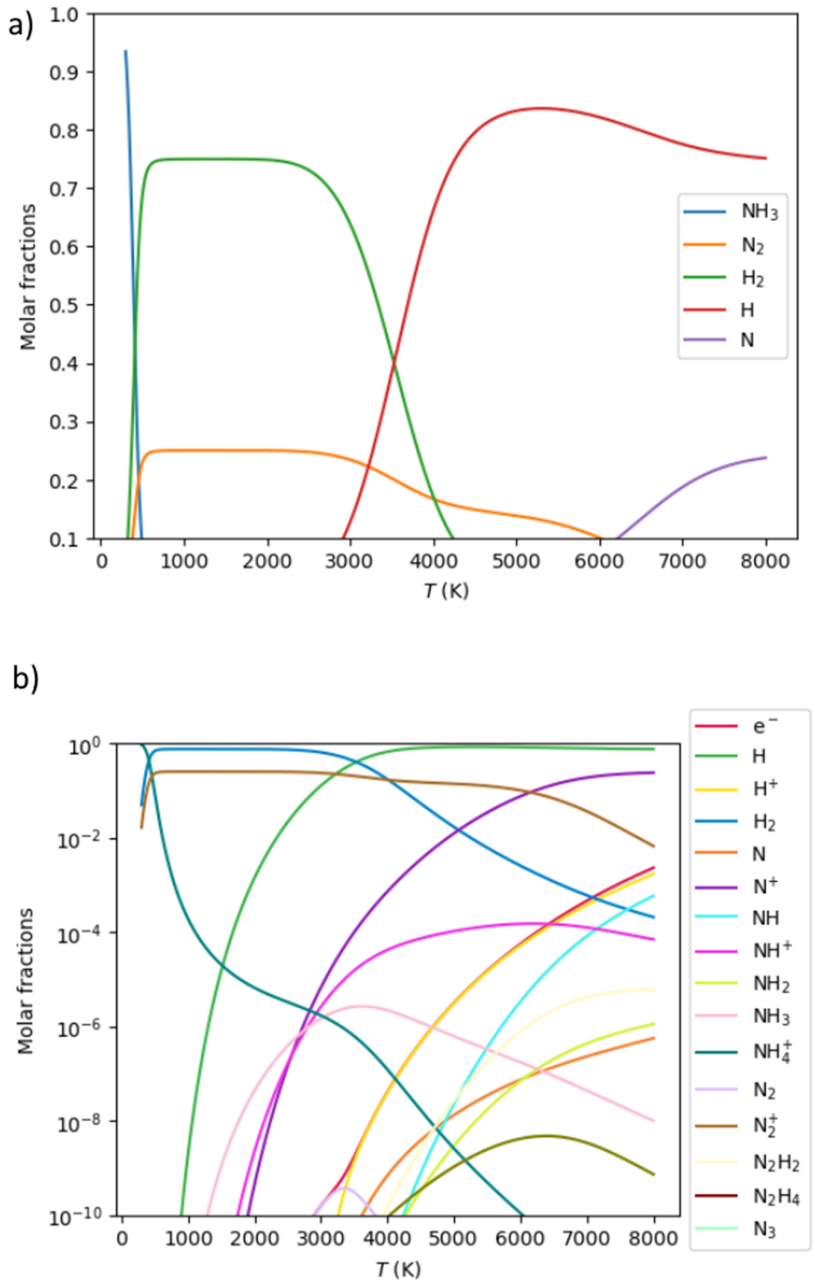


Figure S3. Thermodynamic equilibrium molar fractions as a function of temperature, on a linear scale (a, showing only the dominant species) and a logarithmic scale (b, presenting also the minor species).

## S.3. Viscosity comparison

The viscosity used in our work is shown together with the calculations by Colombo et al. for pure Nitrogen plasma.

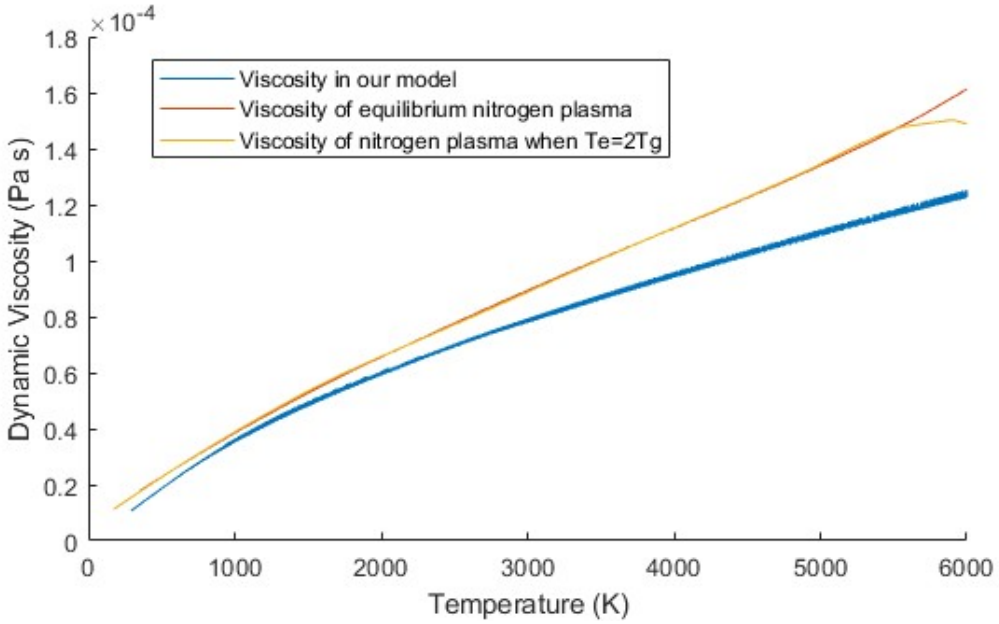


Figure S4. Viscosity used in our work (blue) compared to the values of a pure nitrogen plasma as calculated by Colombo et al.[5]

As one can see, the viscosity we used closely aligns with the more involved plasma viscosities calculated by Colombo et al. The small deviation is caused by the contribution of the hydrogen fraction in the plasma mixture.

## S.4. Full and reduced chemistry set

Table S2 lists all chemical reactions, and their rate coefficients, as well as the corresponding references, for the complete thermal $NH_3$ set, which is used to obtain the reduced chemistry set, and the latter is summarized in Table S3, for the operating conditions of the warm plasma pin-to-pin reactor. For both sets all reactions are detailed balanced, see Maerivoet et al. for further information[6] For other plasma types, it is important to start again from the full set, as the chemistry reduction depends on certain parameters specific for each plasma reactor (such as maximum temperature, quenching rate, residence time…). The reduction method is similar to the one in Maerivoet et al.[6] and is described in section S.5. The reactions that are part of the reduced chemistry set, are also indicated in Table S2 in bold and with asterisk (*).

Table S2 Full set of chemical reactions, their rate coefficients and corresponding references. The reactions present in the reduced chemistry set are indicated in bold and with asterisk. The units of the rate coefficients are also denoted. NNH is included as a species, but it is removed in the reduced set and replaced by $N_2$ + H.

| Reaction | Rate coefficient | Ref. |
|---|---|---|
| **1*) $NH_2 + H (+ M) \rightleftharpoons NH_3 (+ M)$** | See rate equation in footnote [a], with:<br>$k_0 = 3.0 \times 10^{10} \cdot \left(\frac{T_g}{1K}\right)^{-1.9} \frac{m^6}{mol^2 s}$<br>$k_\infty = 1.5 \times 10^{8} \cdot \left(\frac{T_g}{1K}\right)^{0.167} \frac{m^3}{mol\ s}$<br>$F_c = 0.5$<br>$N_{2\ eff} = 2.5$ | 7 |
| **2*) $NH_3 + H \rightleftharpoons NH_2 + H_2$** | $5.4 \times 10^{-1} \cdot \left(\frac{T_g}{1K}\right)^{2.4} \cdot exp\left(\frac{-4.149 \times 10^4\ \mathrm{J/mol}}{R_{const} \cdot T_g}\right) \frac{m^3}{mol\ s}$ | 8 |
| **3*) $NH + H + M \rightleftharpoons NH_2 + M$** | $1.2 \times 10^{13} \cdot \left(\frac{T_g}{1K}\right)^{-2.71} \frac{m^6}{mol^2\ s}$ | 9 |
| **4*) $NH_2 + H \rightleftharpoons NH + H_2$** | $5.1 \times 10^{2} \cdot \left(\frac{T_g}{1K}\right)^{1.5} \cdot exp\left(\frac{-1.548 \times 10^4\ \mathrm{J/mol}}{R_{const} \cdot T_g}\right) \frac{m^3}{mol\ s}$ | 7 |
| **5*) $NH_2 + NH_2 \rightleftharpoons NH_3 + NH$** | $5.6 \times 10^{-6} \cdot \left(\frac{T_g}{1K}\right)^{3.53} \cdot exp\left(\frac{-2.310\ \times 10^3\ \mathrm{J/mol}}{R_{const} \cdot T_g}\right) \frac{m^3}{mol\ s}$ | 10 |
| 6) $NH_2 + NH_2 \rightleftharpoons t\text{-}N_2H_2 + H_2$ | $1.7 \times 10^{2} \cdot \left(\frac{T_g}{1K}\right)^{1.02} \cdot exp\left(\frac{-49.3\ \times 10^3\ \mathrm{J/mol}}{R_{const} \cdot T_g}\right) \frac{m^3}{mol\ s}$ | 10 |
| 7) $NH_2 + NH_2 \rightleftharpoons H_2NN + H_2$ | $7.2 \times 10^{-2} \cdot \left(\frac{T_g}{1K}\right)^{1.88} \cdot exp\left(\frac{-36.83\ \times 10^3\ \mathrm{J/mol}}{R_{const} \cdot T_g}\right) \frac{m^3}{mol\ s}$ | 10 |
| 8) $NH_2 + NH_2 (+ M) \rightleftharpoons N_2H_4 (+ M)$ | See rate equation in footnote [a], with:<br>$k_0 = 1.6 \times 10^{22} \cdot \left(\frac{T_g}{1K}\right)^{-5.49} \cdot exp\left(\frac{-8.31\ \times 10^3\ \mathrm{J/mol}}{R_{const} \cdot T_g}\right) \frac{m^6}{mol^2 s}$<br>$k_\infty = 5.6 \times 10^{8} \cdot \left(\frac{T_g}{1K}\right)^{-0.414} \cdot exp\left(\frac{-276\ \mathrm{J/mol}}{R_{const} \cdot T_g}\right) \frac{m^3}{mol\ s}$<br>$F_c = 0.31$ | 10 |
| **9*) $NH_2 + NH \rightleftharpoons t\text{-}N_2H_2 + H$** | $1.2 \times 10^{9} \cdot \left(\frac{T_g}{1K}\right)^{-0.5} \frac{m^3}{mol\ s}$ | 11 |
| **10*) $NH_2 + NH \rightleftharpoons c\text{-}N_2H_2 + H$** | $3.0 \times 10^{8} \cdot \left(\frac{T_g}{1K}\right)^{-0.5} \frac{m^3}{mol\ s}$ | 11 |
| **11*) $NH_2 + NH \rightleftharpoons NH_3 + N$** | $9.6 \times 10^{-3} \cdot \left(\frac{T_g}{1K}\right)^{2.46} \cdot exp\left(\frac{-4.477 \times 10^2\ J/mol}{R_{const} \cdot T_g}\right) \frac{m^3}{mol\ s}$ | 10 |
| **12*) $NH_2 + N \rightleftharpoons N_2 + H + H$** | $7 \times 10^{7} \frac{m^3}{mol\ s}$ | 12 |
| 13) $NH + M \rightleftharpoons N + H + M$ | $1.8 \times 10^{8} \cdot exp\left(\frac{-313 \times 10^3\ J/mol}{R_{const} \cdot T_g}\right) \frac{m^3}{mol\ s}$ | 9 |
| 14) $NH + H \rightleftharpoons N + H_2$ | $3.49 \times 10^{7} \cdot \left(\frac{T_g}{1K}\right)^{-0.52} \cdot exp\left(\frac{-144 \times 10^3\ J/mol}{R_{const} \cdot T_g}\right) \frac{m^3}{mol\ s}$ | 13 |
| **15*) $NH + NH \rightleftharpoons NNH + H$** | $6.2 \times 10^{7} \cdot \left(\frac{T_g}{1K}\right)^{-0.036} \cdot exp\left(\frac{6.736 \times 10^2\ J/mol}{R_{const} \cdot T_g}\right) \frac{m^3}{mol\ s}$ | 10 |
| 16) $NH + NH \rightleftharpoons NH_2 + N$ | $5.7 \times 10^{-7} \cdot \left(\frac{T_g}{1K}\right)^{3.88} \cdot exp\left(\frac{-1.430 \times 10^3\ J/mol}{R_{const} \cdot T_g}\right) \frac{m^3}{mol\ s}$ | 10 |
| **17*) $NH + N \rightleftharpoons N_2 + H$** | $1.17 \times 10^{7} \cdot \left(\frac{T_g}{1K}\right)^{0.51} \cdot exp\left(\frac{-80\ \mathrm{J/mol}}{R_{const} \cdot T_g}\right) \frac{m^3}{mol\ s}$ | 14 |

| | | |
|---|---|---|
| **18*) $H_2 + M \rightleftharpoons H + H + M$** | $4.6 \times 10^{13} \cdot \left(\frac{T_g}{1K}\right)^{-1.4} \cdot exp\left(\frac{-4.367 \times 10^5\ J/mol}{R_{const} \cdot T_g}\right) \frac{m^3}{mol\ s}$<br>$H_{2\ eff} = 2.5$ | 15 |
| 19) $N_2H_3 + H (+ M) \rightleftharpoons N_2H_4 (+ M)$ | See rate equation in footnote [a], with:<br>$k_0 = 3.6 \times 10^{10} \cdot \left(\frac{T_g}{1K}\right)^{-1.76} \frac{m^6}{mol^2 s}$<br>$k_\infty = 1.6 \times 10^8 \frac{m^3}{mol\ s}$<br>$F_c = 0.5$ | 7 |
| 20) $N_2H_4 + H \rightleftharpoons N_2H_3 + H_2$ | $2.7 \times 10^{13} \cdot \left(\frac{T_g}{1K}\right)^{2.56} \cdot exp\left(\frac{-5.1 \times 10^3\ J/mol}{R_{const} \cdot T_g}\right) \frac{m^3}{mol\ s}$ | 16 |
| 21) $N_2H_4 + NH_2 \rightleftharpoons N_2H_3 + NH_3$ | $2 \times 10^{-5} \cdot \left(\frac{T_g}{1K}\right)^{3.62} \cdot exp\left(\frac{1.66 \times 10^3\ J/mol}{R_{const} \cdot T_g}\right) \frac{m^3}{mol\ s}$ | 17 |
| **22*) $N_2H_3 (+ M) \rightleftharpoons t\text{-}N_2H_2 + H (+ M)$** | See rate equation in footnote [b], with:<br>$k_0 = 3.8 \times 10^{34} \cdot \left(\frac{T_g}{1K}\right)^{-6.88} \cdot exp\left(\frac{-2.279 \times 10^5 J/mol}{R_{const} \cdot T_g}\right) \frac{m^3}{mol\ s}$<br>$k_\infty = 1.3 \times 10^{11} \cdot \left(\frac{T_g}{1K}\right)^{0.819} \cdot exp\left(\frac{-2.011 \times 10^5\ J/mol}{R_{const} \cdot T_g}\right) \frac{1}{s}$<br>$F_c = (1 - 0.168) \cdot exp\left(\frac{-T_g}{80000\ \mathrm{K}}\right)$<br>$+ 0.168 \cdot exp\left(\frac{-T_g}{28\ \mathrm{K}}\right) + exp\left(\frac{-7298\ \mathrm{K}}{T_g}\right)$<br>$N_{2\ eff} = 2$ | 18 |
| 23) $N_2H_3 + H \rightleftharpoons t\text{-}N_2H_2 + H_2$ | $4.6 \times 10^{-5} \cdot \left(\frac{T_g}{1K}\right)^{3.53} \cdot exp\left(\frac{-15.69 \times 10^3\ J/mol}{R_{const} \cdot T_g}\right) \frac{m^3}{mol\ s}$ | 19 |
| 24) $N_2H_3 + H \rightleftharpoons c\text{-}N_2H_2 + H_2$ | $2.7 \times 10^{-4} \cdot \left(\frac{T_g}{1K}\right)^{3.18} \cdot exp\left(\frac{-27.7 \times 10^3\ J/mol}{R_{const} \cdot T_g}\right) \frac{m^3}{mol\ s}$ | 19 |
| 25) $N_2H_3 + H \rightleftharpoons H_2NN + H_2$ | $3.1 \times 10^{0} \cdot \left(\frac{T_g}{1K}\right)^{2.11} \cdot exp\left(\frac{-9.54 \times 10^2\ J/mol}{R_{const} \cdot T_g}\right) \frac{m^3}{mol\ s}$ | 19 |
| **26*) $N_2H_3 + H \rightleftharpoons NH_2 + NH_2$** | $1.0 \times 10^8 \frac{m^3}{mol\ s}$ | 19 |
| 27) $N_2H_3 + NH_2 \rightleftharpoons t\text{-}N_2H_2 + NH_3$ | $6.1 \times 10^{-7} \cdot \left(\frac{T_g}{1K}\right)^{3.574} \cdot exp\left(\frac{-5 \times 10^3\ J/mol}{R_{const} \cdot T_g}\right) \frac{m^3}{mol\ s}$ | 18 |
| 28) $N_2H_3 + NH_2 \rightleftharpoons H_2NN + NH_3$ | $1.1 \times 10^{-5} \cdot \left(\frac{T_g}{1K}\right)^{3.080} \cdot exp\left(\frac{-8.83 \times 10^2\ J/mol}{R_{const} \cdot T_g}\right) \frac{m^3}{mol\ s}$ | 18 |
| 29) $N_2H_3 + NH \rightleftharpoons t\text{-}N_2H_2 + NH_2$ | $2 \times 10^7 \frac{m^3}{mol\ s}$ | 7 |
| **30*) $t\text{-}N_2H_2 \rightleftharpoons c\text{-}N_2H_2$ £ (twisting)** | See rate equation in footnote [b], with:<br>$k_0 = 2.3 \times 10^{23} \cdot \left(\frac{T_g}{1K}\right)^{-4} \cdot exp\left(\frac{-2.515 \times 10^5\ J/mol}{R_{const} \cdot T_g}\right) \frac{m^3}{mol\ s}$<br>$k_\infty = 1.5 \times 10^8 \cdot exp\left(\frac{-2.30 \times 10^5 J/mol}{R_{const} \cdot T_g}\right) \frac{1}{s}$<br>$F_c = (1 - 0.35) \cdot exp\left(\frac{-T_g}{650\ \mathrm{K}}\right) + 0.35 \cdot exp\left(\frac{-T_g}{10600\ \mathrm{K}}\right)$ | 19 |
| **31*) $t\text{-}N_2H_2 (+ M) \rightleftharpoons c\text{-}N_2H_2 (+ M)$ (bending)** | See rate equation in footnote [b], with:<br>$k_0 = 3.0 \times 10^{22} \cdot \left(\frac{T_g}{1K}\right)^{-3.56} \cdot exp\left(\frac{-2.347 \times 10^5\ J/mol}{R_{const} \cdot T_g}\right) \frac{m^3}{mol\ s}$ | 19 |

| | | |
|---|---|---|
| | $k_\infty = 4.9 \times 10^9 \cdot \left(\frac{T_g}{1K}\right)^{1.18} \cdot exp\left(\frac{-1.996 \times 10^5 J/mol}{R_{const} \cdot T_g}\right)\frac{1}{s}$<br>$F_c = (1 - 0.35) \cdot exp\left(\frac{-T_g}{650\ \mathrm{K}}\right) + 0.35 \cdot exp\left(\frac{-T_g}{10600\ \mathrm{K}}\right)$ | |
| **32*) t-$N_2H_2$ + H ⇌ NNH + $H_2$** | $9.6 \times 10^1 \cdot \left(\frac{T_g}{1K}\right)^{1.8} \cdot exp\left(\frac{-3.766 \times 10^3 J/mol}{R_{const} \cdot T_g}\right)\frac{m^3}{mol\ s}$ | 19 |
| **33*) t-$N_2H_2$ + $NH_2$ ⇌ NNH + $NH_3$** | $2.7 \times 10^{-1} \cdot \left(\frac{T_g}{1K}\right)^{2.226} \cdot exp\left(\frac{4.326 \times 10^3 J/mol}{R_{const} \cdot T_g}\right)\frac{m^3}{mol\ s}$ | 18 |
| **34*) t-$N_2H_2$ + NH ⇌ NNH + $NH_2$** | $2.4 \times 10^0 \cdot \left(\frac{T_g}{1K}\right)^{2.0} \cdot exp\left(\frac{5 \times 10^3 J/mol}{R_{const} \cdot T_g}\right)\frac{m^3}{mol\ s}$ | 20 |
| **35*) c-$N_2H_2$ (+ M) ⇌ NNH + H (+ M)** | See rate equation in footnote [b], with:<br>$k_0 = 9.6 \times 10^{29} \cdot \left(\frac{T_g}{1K}\right)^{-5.44} \cdot exp\left(\frac{-2.674 \times 10^5 J/mol}{R_{const} \cdot T_g}\right)\frac{m^3}{mol\ s}$<br>$k_\infty = 5.7 \times 10^{16} \cdot exp\left(\frac{-2.456 \times 10^5\ J/mol}{R_{const} \cdot T_g}\right)\frac{1}{s}$<br>$F_c = (1 - 0.44) \cdot exp\left(\frac{-T_g}{520\ \mathrm{K}}\right) + 0.44 \cdot exp\left(\frac{-T_g}{6150\ \mathrm{K}}\right)$ | 19 |
| **36*) c-$N_2H_2$ + H ⇌ NNH + $H_2$** | $2.8 \times 10^2 \cdot \left(\frac{T_g}{1K}\right)^{1.720} \cdot exp\left(\frac{-1.966 \times 10^3 J/mol}{R_{const} \cdot T_g}\right)\frac{m^3}{mol\ s}$ | 19 |
| 37) c-$N_2H_2$ + H ⇌ t-$N_2H_2$ + H | $7.8 \times 10^2 \cdot \left(\frac{T_g}{1K}\right)^{1.58} \cdot exp\left(\frac{-9.12 \times 10^3 J/mol}{R_{const} \cdot T_g}\right)\frac{m^3}{mol\ s}$ | 19 |
| 38) $H_2NN$ ⇌ NNH + H | $3.4 \times 10^{18} \cdot \left(\frac{T_g}{1K}\right)^{-4.83} \cdot exp\left(\frac{-1.93 \times 10^5 J/mol}{R_{const} \cdot T_g}\right)\frac{m^3}{mol\ s}$ | 20 |
| **39*) $H_2NN$ ⇌ $N_2$ + $H_2$** | $2.5 \times 10^{14} \cdot exp\left(\frac{-2.209 \times 10^5}{R_{const} \cdot T_g}\right)\frac{1}{s}$ | 21 |
| 40) $H_2NN$ + H ⇌ NNH + $H_2$ | $4.8 \times 10^2 \cdot \left(\frac{T_g}{1K}\right)^{1.5} \cdot exp\left(\frac{3.74 \times 10^3 J/mol}{R_{const} \cdot T_g}\right)\frac{m^3}{mol\ s}$ | 20 |
| 41) $H_2NN$ + H ⇌ t-$N_2H_2$ + H | $7.0 \times 10^7 \frac{m^3}{mol\ s}$ | 20 |
| 42) $H_2NN$ + $NH_2$ ⇌ NNH + $NH_3$ | $1.8 \times 10^0 \cdot \left(\frac{T_g}{1K}\right)^{1.94} \cdot exp\left(\frac{4.82 \times 10^3 J/mol}{R_{const} \cdot T_g}\right)\frac{m^3}{mol\ s}$ | 20 |
| 43) NNH ⇌ $N_2$ + H | $6.35 \times 10^7 \cdot \left(\frac{T_g}{298K}\right)^{-0.53} \cdot exp\left(\frac{1.18 \times 10^5 J/mol}{R_{const} \cdot T_g}\right)\frac{m^3}{mol\ s}$ | 14 |
| 44) NNH + H ⇌ $N_2$ + $H_2$ | $3.99 \times 10^7 \cdot \left(\frac{T_g}{298K}\right)^{0.17} \frac{m^3}{mol\ s}$ | 22 |
| 45) NNH + NH ⇌ $N_2$ + $NH_2$ | $5 \times 10^7 \frac{m^3}{mol\ s}$ | 7 |
| 46) NNH + $NH_2$ ⇌ $N_2$ + $NH_3$ | $5 \times 10^7 \frac{m^3}{mol\ s}$ | 7 |
| **47*) t-$N_2H_2$ (+ M) ⇌ NNH + H (+ M)** | See rate equation in footnote [b], with:<br>$k_0 = 8.7 \times 10^{33} \cdot \left(\frac{T_g}{1K}\right)^{-6.91} \cdot exp\left(\frac{-2.946 \times 10^5 J/mol}{R_{const} \cdot T_g}\right)\frac{m^3}{mol\ s}$<br>$k_\infty = 6.3 \times 10^{16} \cdot exp\left(\frac{-2.678 \times 10^5}{R_{const} \cdot T_g}\right)\frac{1}{s}$<br>$F_c = (1 - 0.44) \cdot exp\left(\frac{-T_g}{520\ \mathrm{K}}\right) + 0.44 \cdot exp\left(\frac{-T_g}{6150\ \mathrm{K}}\right)$ | 19 |

| | | |
|---|---|---|
| 48) $N_2H_4 + M \rightleftharpoons H_2NN + H_2 + M$ | PLOG rate (see [20]):<br>$k_{0.1\text{bar}} = 4 \times 10^{38} \cdot \left(\frac{T_g}{1K}\right)^{-9.85} \cdot exp\left(\frac{-3 \times 10^5 J/mol}{R_{const} \cdot T_g}\right)\frac{m^3}{mol\ s}$<br>$k_{1\text{bar}} = 5.3 \times 10^{33} \cdot \left(\frac{T_g}{1K}\right)^{-8.35} \cdot exp\left(\frac{-2.9 \times 10^5 J/mol}{R_{const} \cdot T_g}\right)\frac{m^3}{mol\ s}$<br>$k_{10\text{bar}} = 2.5 \times 10^{33} \cdot \left(\frac{T_g}{1K}\right)^{-8.2} \cdot exp\left(\frac{-2.9 \times 10^5 J/mol}{R_{const} \cdot T_g}\right)\frac{m^3}{mol\ s}$ | 20 |
| **49*) $N_2H_4 + H \rightleftharpoons NH_3 + NH_2$** | $3.0 \times 10^0 \cdot \left(\frac{T_g}{1K}\right)^{2.070} \cdot exp\left(\frac{-3.352 \times 10^4}{R_{const} \cdot T_g}\right)\frac{m^3}{mol\ s}$ | 17 |
| **50*) $N_2 + M \rightleftharpoons N + N + M$** | $3.0 \times 10^{10} \cdot exp\left(\frac{-9.412 \times 10^5\ J/mol}{R_{const} \cdot T_g}\right) \cdot \left(1 - exp\left(\frac{-2.789 \times 10^4\ J/mol}{R_{const} \cdot T_g}\right)\right)\frac{m^3}{mol\ s}$<br>$N_{2\,eff} = 2.2$ | 23 |

[a] NNH in these reactions was substituted for $N_2$ and H, as discussed in the main paper

[b] Notes: a falloff expression, Lindemann-Hinshelwood expression with broadening factor:

$$k = \frac{k_0[M]k_\infty}{k_0[M] + k_\infty}F; \log F = \frac{\log F_c}{1 + \left[\frac{\log(k_0[M]/k_\infty)}{N}\right]^2}; N = 0.75 - 1.27 \log F_c$$

Table S3 Reduced set of chemical reactions, their rate coefficients and corresponding references. The units of the rate coefficients are also denoted. NNH is replaced by $N_2$ + H as a species.

| Reaction | Rate coefficient | Ref. |
|---|---|---|
| 1) $NH_2 + H (+ M) \rightleftharpoons NH_3 (+ M)$ | See rate equation in footnote [a], with:<br>$k_0 = 3.0 \times 10^{10} \cdot \left(\frac{T_g}{1K}\right)^{-1.9} \frac{m^6}{mol^2 s}$<br>$k_\infty = 1.5 \times 10^{8} \cdot \left(\frac{T_g}{1K}\right)^{0.167} \frac{m^3}{mol\ s}$<br>$F_c = 0.5$<br>$N_{2\,eff} = 2.5$ | 7 |
| 2) $NH_3 + H \rightleftharpoons NH_2 + H_2$ | $5.4 \times 10^{-1} \cdot \left(\frac{T_g}{1K}\right)^{2.4} \cdot exp\left(\frac{-4.149 \times 10^4\ \mathrm{J/mol}}{R_{const} \cdot T_g}\right) \frac{m^3}{mol\ s}$ | 8 |
| 3) $NH + H + M \rightleftharpoons NH_2 + M$ | $1.2 \times 10^{13} \cdot \left(\frac{T_g}{1K}\right)^{-2.71} \frac{m^6}{mol^2\ s}$ | 9 |
| 4) $NH_2 + H \rightleftharpoons NH + H_2$ | $5.1 \times 10^{2} \cdot \left(\frac{T_g}{1K}\right)^{1.5} \cdot exp\left(\frac{-1.548 \times 10^4\ \mathrm{J/mol}}{R_{const} \cdot T_g}\right) \frac{m^3}{mol\ s}$ | 7 |
| 5) $NH_2 + NH_2 \rightleftharpoons NH_3 + NH$ | $5.6 \times 10^{-6} \cdot \left(\frac{T_g}{1K}\right)^{3.53} \cdot exp\left(\frac{-2.310\ \times 10^3\ \mathrm{J/mol}}{R_{const} \cdot T_g}\right) \frac{m^3}{mol\ s}$ | 10 |
| 6) $NH_2 + NH \rightleftharpoons t\text{-}N_2H_2 + H$ | $1.2 \times 10^{9} \cdot \left(\frac{T_g}{1K}\right)^{-0.5} \frac{m^3}{mol\ s}$ | 11 |
| 7) $NH_2 + NH \rightleftharpoons c\text{-}N_2H_2 + H$ | $3.0 \times 10^{8} \cdot \left(\frac{T_g}{1K}\right)^{-0.5} \frac{m^3}{mol\ s}$ | 11 |
| 8) $NH_2 + NH \rightleftharpoons NH_3 + N$ | $9.6 \times 10^{-3} \cdot \left(\frac{T_g}{1K}\right)^{2.46} \cdot exp\left(\frac{-4.477 \times 10^2\ J/mol}{R_{const} \cdot T_g}\right) \frac{m^3}{mol\ s}$ | 10 |
| 9) $NH_2 + N \rightleftharpoons N_2 + H + H$ | $7 \times 10^{7} \frac{m^3}{mol\ s}$ | 12 |
| 10) $NH + NH \rightleftharpoons N_2 + H + H$ [a] | $6.2 \times 10^{7} \cdot \left(\frac{T_g}{1K}\right)^{-0.036} \cdot exp\left(\frac{6.736 \times 10^2\ J/mol}{R_{const} \cdot T_g}\right) \frac{m^3}{mol\ s}$ | 10 |
| 11) $NH + N \rightleftharpoons N_2 + H$ | $6.402 \text{ x } 10^{5} \cdot \left(\frac{T_g}{1K}\right)^{0.51} \cdot exp\left(\frac{-80\ \mathrm{J/mol}}{R_{const} \cdot T_g}\right) \frac{m^3}{mol\ s}$ | 14 |
| 12) $H_2 + M \rightleftharpoons H + H + M$ | $4.6 \times 10^{13} \cdot \left(\frac{T_g}{1K}\right)^{-1.4} \cdot exp\left(\frac{-4.367 \times 10^5\ J/mol}{R_{const} \cdot T_g}\right) \frac{m^3}{mol\ s}$<br>$H_{2\,eff} = 2.5$ | 15 |
| 13)<br>$N_2H_3 (+ M) \rightleftharpoons t\text{-}N_2H_2 + H (+ M)$ | See rate equation in footnote [b], with:<br>$k_0 = 3.8 \times 10^{34} \cdot \left(\frac{T_g}{1K}\right)^{-6.88} \cdot exp\left(\frac{-2.279 \times 10^5 J/mol}{R_{const} \cdot T_g}\right) \frac{m^3}{mol\ s}$<br>$k_\infty = 1.3 \times 10^{11} \cdot \left(\frac{T_g}{1K}\right)^{0.819} \cdot exp\left(\frac{-2.011 \times 10^5\ J/mol}{R_{const} \cdot T_g}\right) \frac{1}{s}$<br>$F_c = (1 - 0.168) \cdot exp\left(\frac{-T_g}{80000\ \mathrm{K}}\right) + 0.168 \cdot exp\left(\frac{-T_g}{28\ \mathrm{K}}\right) + exp\left(\frac{-7298\ \mathrm{K}}{T_g}\right)$<br>$N_{2\,eff} = 2$ | 18 |
| 14) $N_2H_3 + H \rightleftharpoons NH_2 + NH_2$ | $1.0 \times 10^{8} \frac{m^3}{mol\ s}$ | 19 |

| | | |
|---|---|---|
| 15) t-$N_2H_2$ (+ M) ⇌ c-$N_2H_2$ (+ M) | See rate equation in footnote [b], with: $k_0 = 3.0 \times 10^{22} \cdot \left(\frac{T_g}{1K}\right)^{-3.56} \cdot exp\left(\frac{-2.347 \times 10^5\ J/mol}{R_{const} \cdot T_g}\right)\frac{m^3}{mol\ s}$ $k_\infty = 4.9 \times 10^9 \cdot \left(\frac{T_g}{1K}\right)^{1.18} \cdot exp\left(\frac{-1.996 \times 10^5 J/mol}{R_{const} \cdot T_g}\right)\frac{1}{s}$ $F_c = (1 - 0.35) \cdot exp\left(\frac{-T_g}{650\ \mathrm{K}}\right) + 0.35 \cdot exp\left(\frac{-T_g}{10600\ \mathrm{K}}\right)$ | 19 |
| 16) t-$N_2H_2$ + H ⇌ $N_2$ + H + $H_2$ [a] | $9.6 \times 10^1 \cdot \left(\frac{T_g}{1K}\right)^{1.8} \cdot exp\left(\frac{-3.766 \times 10^3 J/mol}{R_{const} \cdot T_g}\right)\frac{m^3}{mol\ s}$ | 19 |
| 17) t-$N_2H_2$ + $NH_2$ ⇌ $N_2$ + H + $NH_3$ [a] | $2.7 \times 10^{-1} \cdot \left(\frac{T_g}{1K}\right)^{2.226} \cdot exp\left(\frac{4.326 \times 10^3 J/mol}{R_{const} \cdot T_g}\right)\frac{m^3}{mol\ s}$ | 18 |
| 18) c-$N_2H_2$ (+ M) ⇌ $N_2$ + H + H [a] (+ M) | See rate equation in footnote [b], with: $k_0 = 9.6 \times 10^{29} \cdot \left(\frac{T_g}{1K}\right)^{-5.44} \cdot exp\left(\frac{-2.674 \times 10^5 J/mol}{R_{const} \cdot T_g}\right)\frac{m^3}{mol\ s}$ $k_\infty = 5.7 \times 10^{16} \cdot exp\left(\frac{-2.456 \times 10^5\ J/mol}{R_{const} \cdot T_g}\right)\frac{1}{s}$ $F_c = (1 - 0.44) \cdot exp\left(\frac{-T_g}{520\ \mathrm{K}}\right) + 0.44 \cdot exp\left(\frac{-T_g}{6150\ \mathrm{K}}\right)$ | 19 |
| 19) c-$N_2H_2$ + H ⇌ $N_2$ + H + $H_2$ [a] | $2.8 \times 10^2 \cdot \left(\frac{T_g}{1K}\right)^{1.720} \cdot exp\left(\frac{-1.966 \times 10^3 J/mol}{R_{const} \cdot T_g}\right)\frac{m^3}{mol\ s}$ | 19 |
| 20) $H_2NN$ ⇌ $N_2$ + $H_2$ | $2.5 \times 10^{14} \cdot exp\left(\frac{-2.209 \times 10^5}{R_{const} \cdot T_g}\right)\frac{1}{s}$ | 20 |
| 21) t-$N_2H_2$ (+ M) ⇌ $N_2$ + H + H (+ M) [a] | See rate equation in footnote [b], with: $k_0 = 8.7 \times 10^{33} \cdot \left(\frac{T_g}{1K}\right)^{-6.91} \cdot exp\left(\frac{-2.946 \times 10^5 J/mol}{R_{const} \cdot T_g}\right)\frac{m^3}{mol\ s}$ $k_\infty = 6.3 \times 10^{16} \cdot exp\left(\frac{-2.678 \times 10^5}{R_{const} \cdot T_g}\right)\frac{1}{s}$ $F_c = (1 - 0.44) \cdot exp\left(\frac{-T_g}{520\ \mathrm{K}}\right) + 0.44 \cdot exp\left(\frac{-T_g}{6150\ \mathrm{K}}\right)$ | 19 |
| 22) $N_2H_4$ + H ⇌ $NH_3$ + $NH_2$ | $3.0 \times 10^0 \cdot \left(\frac{T_g}{1K}\right)^{2.070} \cdot exp\left(\frac{-3.352 \times 10^4}{R_{const} \cdot T_g}\right)\frac{m^3}{mol\ s}$ | 17 |
| 23) $N_2$ + M ⇌ N + N + M | $3.0 \times 10^{10} \cdot exp\left(\frac{-9.412 \times 10^5\ J/mol}{R_{const} \cdot T_g}\right) \cdot \left(1 - exp\left(\frac{-2.789 \times 10^4\ J/mol}{R_{const} \cdot T_g}\right)\right)\frac{m^3}{mol\ s}$ $N_{2\,eff} = 2.2$ | 23 |

[a] NNH in these reactions was substituted for $N_2$ and H, as discussed in the text.

[b] Notes: a falloff expression, Lindemann-Hinshelwood expression with broadening factor:

$$k = \frac{k_0[M]k_\infty}{k_0[M] + k_\infty}F; \log F = \frac{\log F_c}{1 + \left[\frac{\log(k_0[M]/k_\infty)}{N}\right]^2}; N = 0.75 - 1.27 \log F_c$$

# S.5. Chemistry reduction

### S.5.1. Methodology

The full workflow is shown in figure S5. We ran multiple simulations with a 0D model for an extensive gas temperature range (1200 K to 6000 K) and an extensive range of starting conditions (ranging from pure $NH_3$ to diluted $NH_3$, i.e., 10 % $NH_3$ in 90 % $N_2$ or 10 % $NH_3$ in 90 % $H_2$), see top of the figure. We incorporate temperatures up to 6000 K in our initial reduction of the $NH_3$ chemistry, so that our chemical kinetics scheme is valid in the entire range. As can be seen in the main manuscript, in Figure 7, almost all $NH_3$ conversion will occur between a temperature range of 2400 to 3000 K, and thus, any decomposition of 100 % $NH_3$ with a starting temperature of 3200 K or higher does not reflect a real location in the pin-to-pin reactor under these conditions. Instead, we do this to allow the reduced model to be applicable for other reactors, which might heat $NH_3$ faster, so that the $NH_3$ gas could reach higher temperatures.

In each iteration, we omitted a single reaction from the reaction kinetics set and we calculated the deviation on the output, as the effect of omitting this one single reaction on the full unmodified set. The deviation is the maximum difference between the original set and the single reaction reduced set at any point in time for each species. For instance, reactions Q, R, S and T could have deviations y, x, z and w, respectively. After each reaction receives a deviation score, they are sorted from least important (lowest score) to most important (highest score). So, if $w < x < y < z$, then we sort their impact as $T < R < Q < S$. Finally, we run additional simulations, removing multiple reactions based on the previous sorted deviation scores, from low impact to high. Four groups might then be identified, i.e., 1. “only T removed as least impactful”, 2. “R and T removed as the two least impactful”, etc. This leaves 50 sets of simulations for various conditions, each with one more reaction omitted than the previous one. The final reduced set is chosen based on the maximum allowed deviation at any point in the simulation compared to the full, unmodified set, which was set in this case to have an absolute deviation of 0.1 %. In the example case, if the simulation ran without T and R would yield a deviation score of 0.08 % and the simulation without Q, T and R would yield 0.12 %, the resulting set would omit species R and T but not Q. Our final reduced set consists of 13 species and 23 reactions.

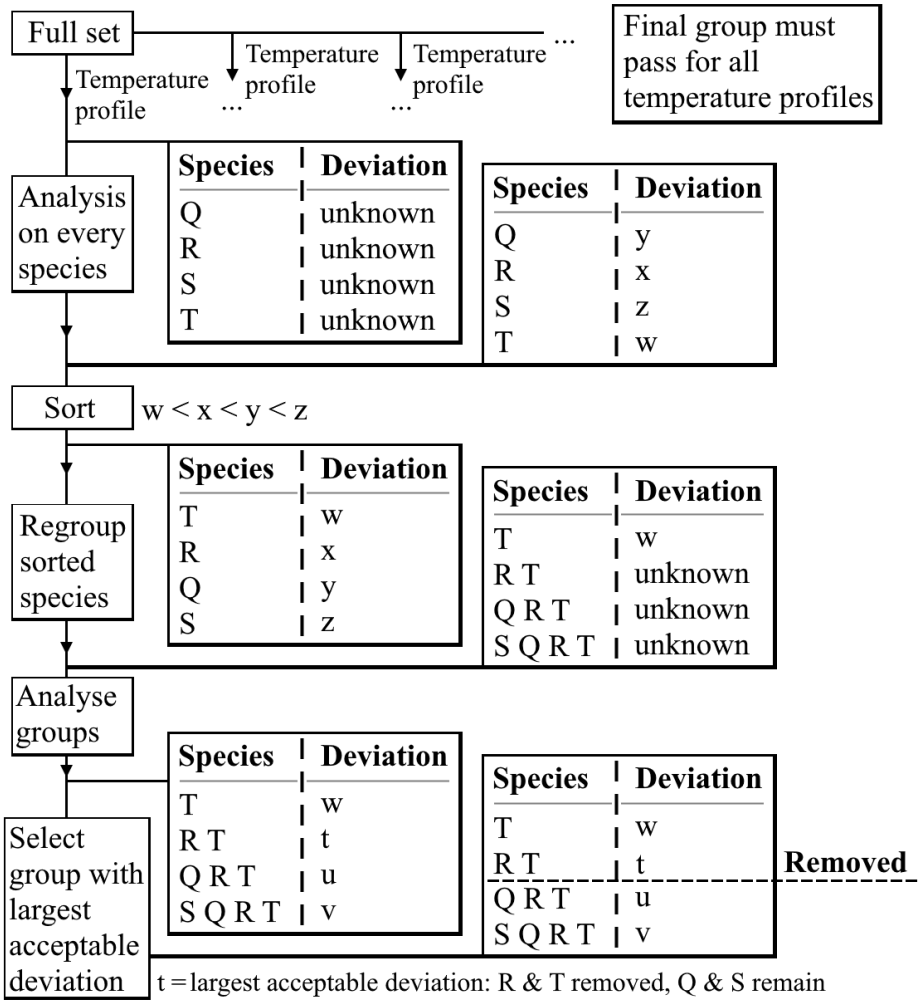


Figure S5. Reduction scheme adapted with permission from Maerivoet et al.[6] depicting the method of reduction for reactions from the full $NH_3$ set shown in Table S2. All rights reserved Elsevier Ltd. ©

In the paper of Maerivoet et al.[6] this reduction was first performed for species, but in our case, the set could not be reduced in terms of species, so all 13 species have to be kept in the reduced set.

This reduced set is not sufficiently stable yet for multi-dimensional modelling. Indeed, as described in numerous papers, NNH is an important intermediate compound for $NH_3$ cracking. However, a low potential energy barrier of 33.5 kJ/mol [24] to $N_2$ and H via tunneling suggests a very short calculated lifetime, in the order of $10^{-8}$-$10^{-10}$ s.[25] In a multi-dimensional model, any species which forms and is immediately destroyed, without any convective or diffusive transport to an adjacent mesh element, results in unwanted numerical instabilities. Therefore, instead of further increasing the number of mesh elements (with mesh size down to the nanometer scale), this species is removed and directly replaced with the unimolecular tunneling products $N_2$ and H. The effect of this change and the reduction on the chemistry is shown below.

### S.5.2. Results

Figure SS6 compares the full and reduced kinetic sets (solid and dashed lines, respectively) following the reduction method for pure $NH_3$ decomposition at 2800 K. As the maximum allowed tolerance is set at 0.1 % absolute deviation of any species to the total molar concentration, no significant difference can be observed in Figure SS6a, which shows the molar concentrations on a linear scale. Figure SS6b depicts the molar concentrations on a logarithmic scale, where differences can be seen for the very low molar concentrations. As any thermodynamic or transport variable depends on the molar concentration of the species, the large relative error observed for the species with low concentrations is negligible for the overall plasma behavior. This is the case as long as the individual properties of a species (enthalpy, entropy, …) do not differ by orders of magnitude from all other species.

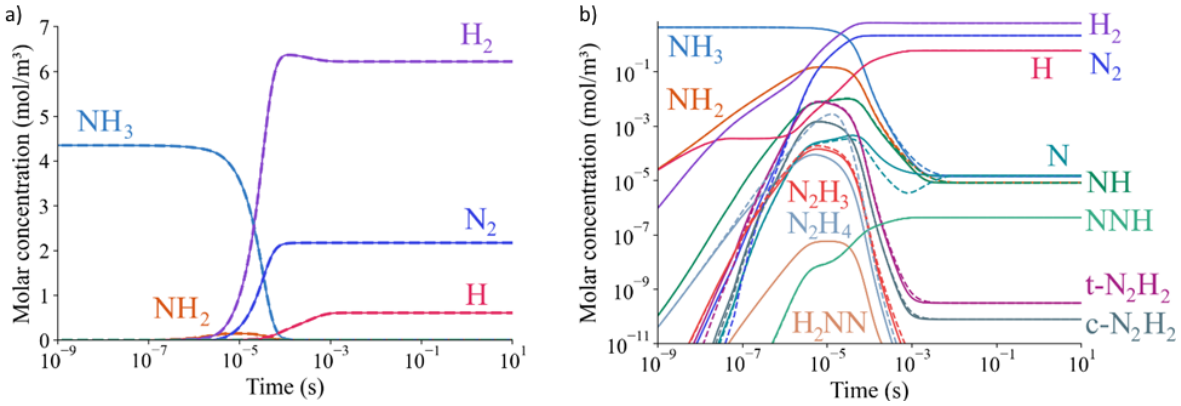


Figure S6. Molar concentration of $NH_3$ and (major) decomposition products, as a function of time at 2800 K, in linear (a) and logarithmic (b) scale. Full lines represent the full kinetic set, while dashed lines represent the reduced kinetic set.

As mentioned above, NNH is removed from the reduced set to avoid numerical instabilities. Figure S7 compares the full and reduced kinetic sets (solid and dashed lines, respectively), with NNH replaced by $N_2$ and H in the reduced set, again for pure $NH_3$ thermal cracking at 2800 K.

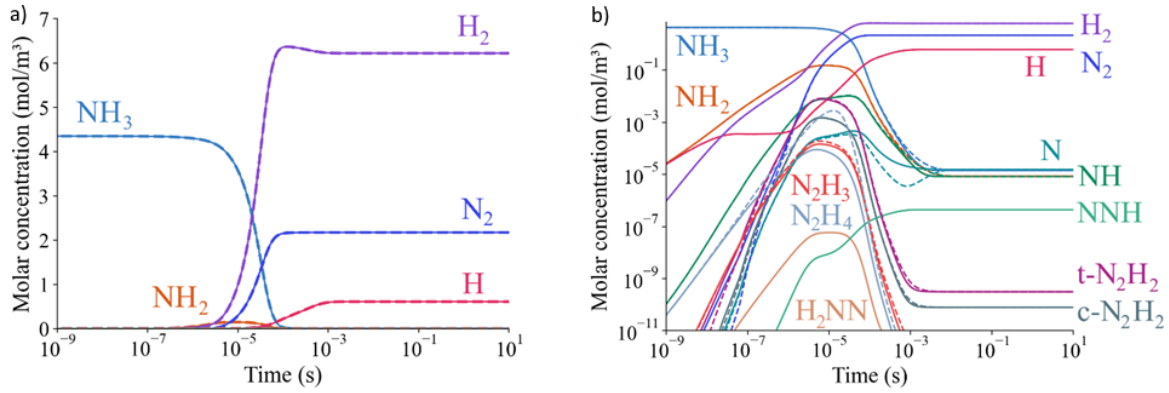


Figure S7. Molar concentration of $NH_3$ and (major) decomposition products, as a function of time at 2800 K, in linear (a) and logarithmic (b) scale. Full lines represent the full kinetic set, while dashed lines represent the reduced kinetic set without NNH.

We can see that the removal of NNH from the reduced set has a negligible effect on the kinetics, although NNH has a larger molar concentration than other intermediate species. This is because the destruction of NNH to $N_2$ and H is extremely fast, and any NNH formed is thus the result

of the detailed balanced reverse rate. The major effect of the chemistry reduction (both with and without NNH in the model) seems to be an overestimation of the $N_2H_4$ concentration by an order of magnitude around 10 µs. This means that we cannot use our reduced model to study the production of $N_2H_4$ in warm plasma, but that is not the purpose of this work. On the other hand, this overestimation has a negligible effect on the thermodynamic properties of the model, as the $N_2H_4$ molar concentration never exceeds $10^{-4}$ mol/m$^3$.

## S.6. Reaction pathway analysis for high SEI

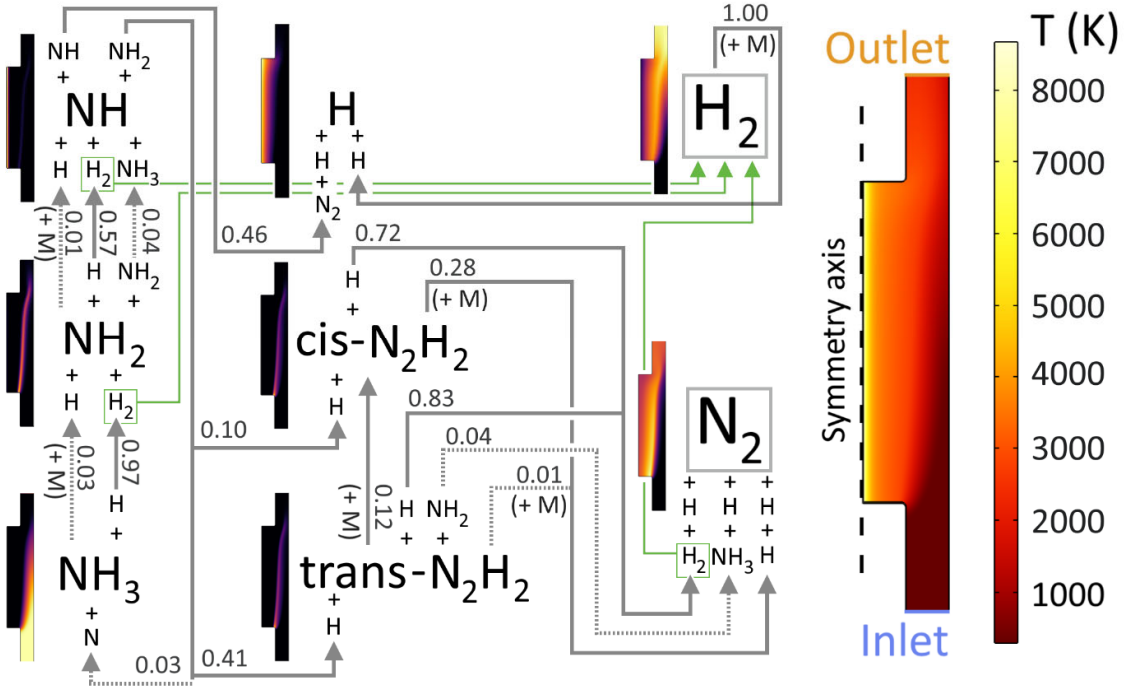


Figure S8. Reaction pathways analysis of $NH_3$ decomposition at 5 NLM, SEI = 231 kJ/mol. The 2D plots illustrate the mole fractions of the species, while the temperature profile is shown on the right. The arrow directions correspond to the net rates of reactions in the complete reactor. The branching ratios for the destruction of a species are denoted next to the arrows, (+ M) is shown if the reaction requires a third body as neutral collision partner to proceed. Reactions contributing to less than 10 % of the species destruction are indicated with a dashed arrow, while reactions contributing less than 1 % are omitted, for clarity. Importantly, all produced (green) $H_2$ molecules are linked to the final $H_2$ product with green arrows.

We have extrapolated our results to a much higher SEI to investigate if the same pathways are utilized in a high-power case. It must be noted that the wall temperature at this SEI is above the melting temperature of quartz glass[26]. There are three main differences between the high SEI case (Figure S8) and low SEI case (Figure 8 in the main paper). First, the decomposition of $NH_3$ to $NH_2$ in Figure 8 happens for 90 % upon reaction with H, while in Figure S8, this contribution becomes 97 %. The higher temperature in the central plasma column and larger temperature gradients at this higher SEI (cf. Figure S8) allow for 40 % more $H_2$ to be dissociated in the plasma center, and because H diffusion is very fast, more H atoms will reach the reactive region at higher SEI, hence the even larger contribution of H atoms to $NH_3$ decomposition. The same holds true, to some extent, for the decomposition of $NH_2$ (i.e., 57% in Figure S8 vs 53% in Figure 8).

Second, the dominant process for NH decomposition has shifted from the reaction to trans-$N_2H_2$ to the direct formation of $N_2$ upon reaction with a second NH radical, although the difference is small (45 vs 39% in Figure 8, and 41 vs 46% in Figure S8). This is an indirect effect of the higher H concentration, i.e., more H causes faster $NH_2$ decomposition, and thus more NH is available to react with NH instead of with $NH_2$.

Third, also the reactions destroying cis-$N_2H_2$ and trans-$N_2H_2$ with H have a somewhat higher contribution (72 and 83%, respectively in Figure S8, vs 62 and 77% in Figure 8), while the reactions with M, $NH_2$ and the isomerization reaction obviously become less important. This is once again due to the higher H fraction in the reactive region, attributed to faster diffusion.

## S.7. Importance of heat source shape

In previous work[6] we used the shape of the heat source as input to the model, and it can be based on measured temperature profiles or derived from light emission shapes corresponding to the plasma region. In this work, we calculated the heat source self-consistently based on the power input and Joule heating. Here we analyze the effect of increasing the width of the heat source, from its very contracted nature originating by Joule heating (as used in this model) to a tube-filling Gaussian profile. The reason for evaluating the heat source shape is because we hypothesize the important role of H atom diffusion. If the plasma core temperature drops significantly (lower than ~3200 K) the production of H atoms is severely limited. This in turn reduces the conversion and increases the EC. The heat source was modeled as a Gaussian with a maximum at the central axis. The total deposited power was kept constant at 405 W for both heat source shapes, i.e., the power deposited by the fully coupled model for 20 NLM and SEI of 27.6 kJ/mol. The radius of the heat source is defined as the half width at half maximum. FigureS9 illustrates how the EC depends on the width of the Gaussian-shaped heat source, compared to our heat source obtained from Joule heating. Up to 1.5 mm width, the EC is more or less independent of the radius, but a larger radius leads to a significantly higher EC.

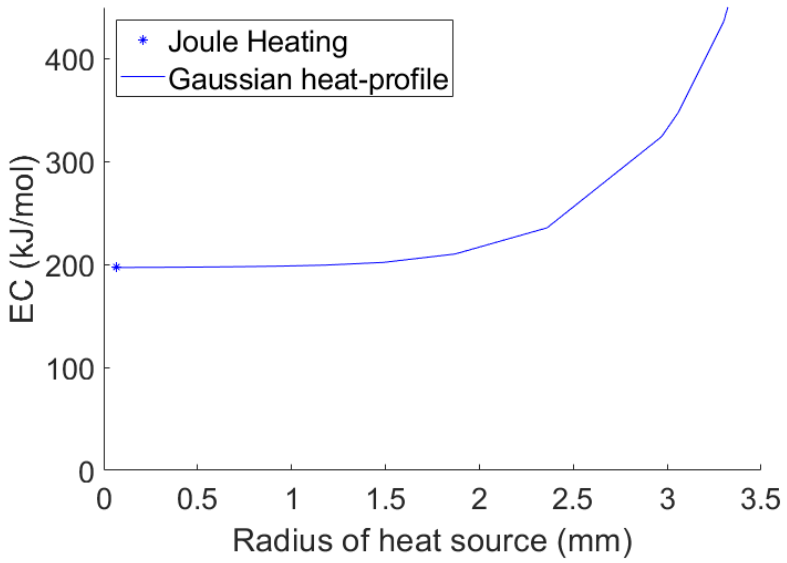

Figure S9. EC as a function of radius of the Gaussian-shaped heat source, and comparison to our heat source obtained from Joule heating, at a flow rate of 15 NLM, SEI of 29 kJ/mol and interelectrode distance of 3 cm.

FigureS10 compares the calculated temperature profiles for a Gaussian heat source width of 0.1 and 1 mm, and clearly explains why the EC (and conversion) remain almost constant when the heat source width is below 2 mm.

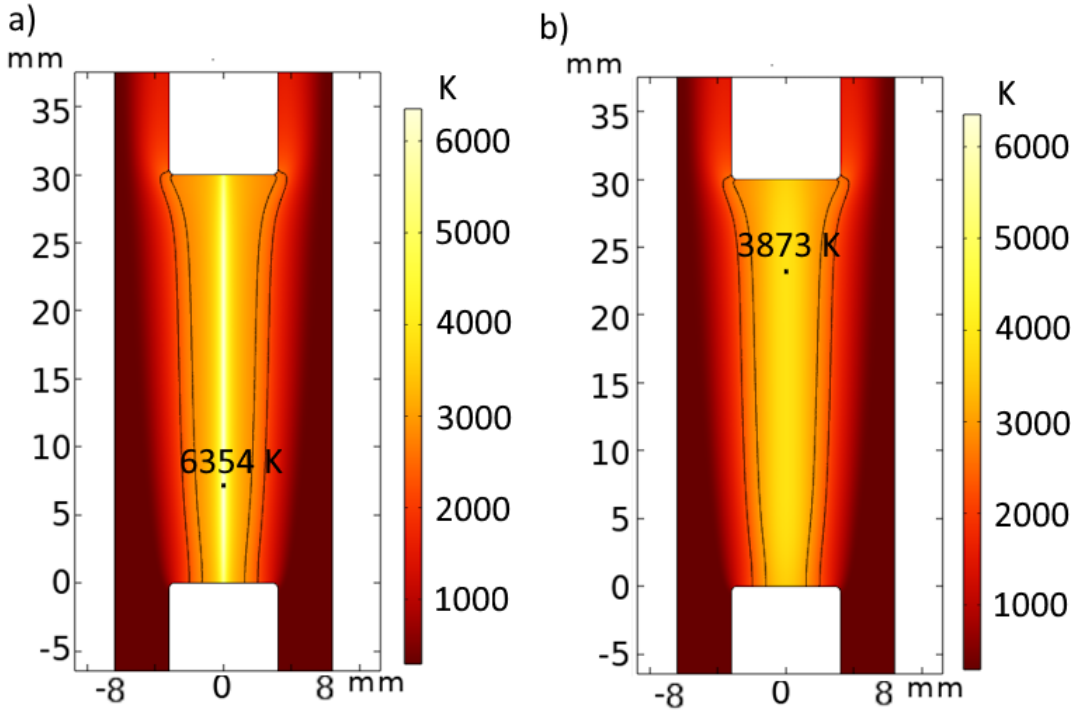


Figure S10. Temperature profile for Gaussian heat source radius of (a) 0.1 mm and (b) 1 mm, at a flow rate of 15 NLM and deposited power of 315 W. The black contour lines indicate the $NH_3$ decomposition rate at 1000 mol/($m^3$s).

Indeed, while the central temperature drops by ca. 40 % for a heat source width of 1 mm vs 0.1 mm (i.e., 3873 K vs 6354 K; cf. Figure S10), the region where the actual chemistry happens remains broadly the same, since the chemically active region is centered around 2700 K. This is because there are no heat losses on the flat tips of the electrodes (boundaries 2 and 10 in Figure S1). Thus, all power that is deposited between r = 0 and 2 mm can only flow outwards by increasing the temperature of the gas surrounding it, or by being stored in high enthalpic products like H atoms, which diffuse away from the hot plasma column. The total amount of H atoms produced in the hot core is lower for the wide plasma (1.1 vs. 0.8 mmol/s), but the difference can still be made up by slightly increasing the maximal temperature of the chemically active zone. This compensation mechanism breaks down when the heat source no longer produces temperatures above 3200 K. This justifies the use of a heat source model, but only in the case where all chemistry happens in the plasma edge and the flow profile in the plasma does not provide a large contribution to species transport.

## S.8. Transport effects 3 and 5 cm interelectrode gap

All unreacted $NH_3$ gas that reaches the chemically active zone must arrive via either diffusion or convection. Figure S11. shows the contribution of diffusion and convection into this zone. The diffusive flux out of this region is negligible and not shown in the figure. The effect of a limited residence time is evident by the fact that there still is a relatively large fraction of $NH_3$ that leaves the reactive zone via convection. i.e. not all gas that enters this zone gets converted. The definition of 'convective in', 'diffusive in' and 'convective out' are given by:

| | |
|---|---|
| Convective in | $\iint_{T=T_c} \vec{v} \cdot \vec{n} \rho \omega_{NH_3} (\vec{v} \cdot \vec{n} > 0) dA$ |
| Diffusive in | $\iint_{T=T_c} \vec{J}_{NH_3} \cdot \vec{n} (\vec{J}_{NH_3} \cdot \vec{n} > 0) dA$ |
| Convective out | $\iint_{T=T_c} \vec{v} \cdot \vec{n} \rho \omega_{NH_3} (\vec{v} \cdot \vec{n} < 0) dA$ |

Where $\vec{J}_{NH_3}$ is defined by equation (22) in the main paper and $\vec{n}$ is the normal on the isotherm with boundary temperature $T_c$ (2400 K).

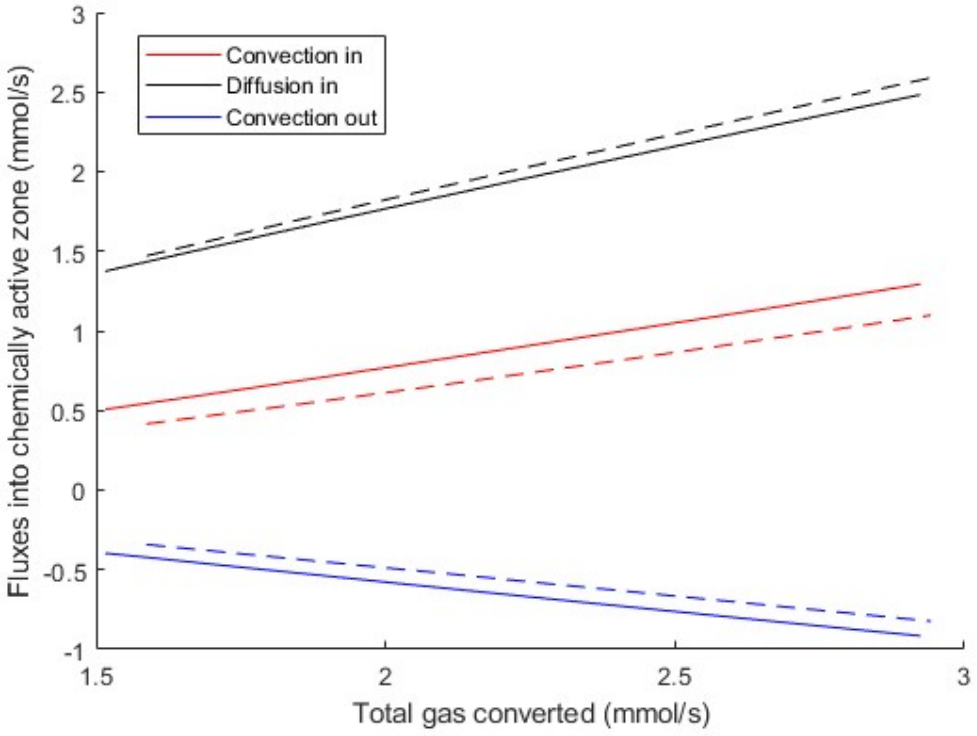


Figure S11. Contribution to total transport of the different components, solid for an interelectrode distance of 3 cm and dashed for an interelectrode distance of 5cm. See legend for color indication. The total flowrate in is 10.8 mmol/s for all cases. Total gas converted increases with increasing SEI, but as

noted in the main paper is the conversion for 3 cm and 5 cm equal for equal SEI. The range in SEI is 27-54 kJ/mol.

Figure S11 shows that a single degree of conversion (same x-position) can be obtained by different fractions of the gas 'flowing' (convective transport) into the chemically active zone (hot region). Secondly it shows the effect of residence time, if the boundary temperature was such that all gas is instantaneously cracked, then the 'convective out' term would be 0. The conversion is thus not solely determined by how much gas flows into the plasma, but by how much gas gets transported into the plasma, via either convection or diffusion.

## References


(1) Churchill, S. W.; Chu, H. H. S. Correlating Equations for Laminar and Turbulent Free Convection from a Horizontal Cylinder. *International Journal of Heat and Mass Transfer* **1975**, *18* (9), 1049–1053. https://doi.org/10.1016/0017-9310(75)90222-7.

(2) COMSOL Multiphysics®. Heat Transfer Module User's Guide, 2023. https://doc.comsol.com/6.2/doc/com.comsol.help.heat/HeatTransferModuleUsersGuide.pdf.

(3) Petrov, V.; Reznik, V. Measurement of the Emissivity of Quartz Glass. *High Temperatures-High Pressures* **1972**, *v. 4*, 687–693.

(4) Naidis, G. V. Simulation of Convection-Stabilized Low-Current Glow and Arc Discharges in Atmospheric-Pressure Air. *Plasma Sources Sci. Technol.* **2007**, *16* (2), 297. https://doi.org/10.1088/0963-0252/16/2/012.

(5) Colombo, V.; Ghedini, E.; Sanibondi, P. Thermodynamic and Transport Properties in Non-Equilibrium Argon, Oxygen and Nitrogen Thermal Plasmas. *Progress in Nuclear Energy* **2008**, *50* (8), 921–933. https://doi.org/10.1016/j.pnucene.2008.06.002.

(6) Maerivoet, S.; Tsonev, I.; Slaets, J.; Reniers, F.; Bogaerts, A. Coupled Multi-Dimensional Modelling of Warm Plasmas: Application and Validation for an Atmospheric Pressure Glow Discharge in CO2/CH4/O2. *Chemical Engineering Journal* **2024**, *492*, 152006. https://doi.org/10.1016/j.cej.2024.152006.

(7) Glarborg, P.; Hashemi, H.; Marshall, P. Challenges in Kinetic Modeling of Ammonia Pyrolysis. *Fuel Communications* **2022**, *10*, 100049. https://doi.org/10.1016/j.jfueco.2022.100049.

(8) Ko, Taeho.; Marshall, Paul.; Fontijn, Arthur. Rate Coefficients for the Hydrogen Atom + Ammonia Reaction over a Wide Temperature Range. *J. Phys. Chem.* **1990**, *94* (4), 1401–1404. https://doi.org/10.1021/j100367a037.

(9) Deppe, J.; Friedrichs, G.; Ibrahim, A.; Römming, H.-J.; Wagner, H. Gg. The Thermal Decomposition of NH2 and NH Radicals. *Berichte der Bunsengesellschaft für physikalische Chemie* **1998**, *102* (10), 1474–1485. https://doi.org/10.1002/bbpc.199800016.

(10) Klippenstein, S. J.; Harding, L. B.; Ruscic, B.; Sivaramakrishnan, R.; Srinivasan, N. K.; Su, M.-C.; Michael, J. V. Thermal Decomposition of NH2OH and Subsequent Reactions: Ab Initio Transition State Theory and Reflected Shock Tube Experiments. *J Phys Chem A* **2009**, *113* (38), 10241–10259. https://doi.org/10.1021/jp905454k.

(11) Davidson, D. F.; Kohse-Höinghaus, K.; Chang, A. Y.; Hanson, R. K. A Pyrolysis Mechanism for Ammonia. *International Journal of Chemical Kinetics* **1990**, *22* (5), 513–535. https://doi.org/10.1002/kin.550220508.

(12) Whyte, A. R.; Phillips, L. F. Rates of Reaction of NH2 with N, NO AND NO2. *Chemical Physics Letters* **1983**, *102* (5), 451–454. https://doi.org/10.1016/0009-2614(83)87444-2.

(13) Li, Z.; Xie, C.; Jiang, B.; Xie, D.; Liu, L.; Sun, Z.; Zhang, D. H.; Guo, H. Quantum and Quasiclassical State-to-State Dynamics of the NH + H Reaction: Competition between Abstraction and Exchange Channels. *The Journal of Chemical Physics* **2011**, *134* (13), 134303. https://doi.org/10.1063/1.3574898.

(14) Caridade, P. J. S. B.; Rodrigues, S. P. J.; Sousa, F.; Varandas, A. J. C. Unimolecular and Bimolecular Calculations for HN2. *J. Phys. Chem. A* **2005**, *109* (10), 2356–2363. https://doi.org/10.1021/jp045102g.

(15) Tsang, W.; Hampson, R. F. Chemical Kinetic Data Base for Combustion Chemistry. Part I. Methane and Related Compounds. *Journal of Physical and Chemical Reference Data* **1986**, *15* (3), 1087–1279. https://doi.org/10.1063/1.555759.

(16) Kanno, N.; Kito, T. Theoretical Study on the Hydrogen Abstraction Reactions from Hydrazine Derivatives by H Atom. *International Journal of Chemical Kinetics* **2020**, *52* (8), 548–555. https://doi.org/10.1002/kin.21370.

(17) Gao, Y.; Alecu, I. M.; Hashemi, H.; Glarborg, P.; Marshall, P. Reactions of Hydrazine with the Amidogen Radical and Atomic Hydrogen. *Proceedings of the Combustion Institute* **2023**, *39* (1), 571–579. https://doi.org/10.1016/j.proci.2022.07.045.

(18) Diévart, P.; Catoire, L. Contributions of Experimental Data Obtained in Concentrated Mixtures to Kinetic Studies: Application to Monomethylhydrazine Pyrolysis. *J. Phys. Chem. A* **2020**, *124* (30), 6214–6236. https://doi.org/10.1021/acs.jpca.0c03144.

(19) Marshall, P.; Rawling, G.; Glarborg, P. New Reactions of Diazene and Related Species for Modelling Combustion of Amine Fuels. *Molecular Physics* **2021**, *119* (17–18), e1979674. https://doi.org/10.1080/00268976.2021.1979674.

(20) Gardiner, W. C. *Gas-Phase Combustion Chemistry*, 2nd ed.; Springer New York: New York, 1999.

(21) Hwang, D.-Y.; Mebel, A. M. Reaction Mechanism of N2/H2 Conversion to NH3: A Theoretical Study. *J. Phys. Chem. A* **2003**, *107* (16), 2865–2874. https://doi.org/10.1021/jp0270349.

(22) Pelevkin, A. V.; Sharipov, A. S. Reactions of Electronically Excited Molecular Nitrogen with H2 and H2O Molecules: Theoretical Study. *Journal of Physics D: Applied Physics* **2018**, *51* (18), 184003. https://doi.org/10.1088/1361-6463/aab97f.

(23) Cejas, E.; Mancinelli, B.; Prevosto, L. Modelling of an Atmospheric–Pressure Air Glow Discharge Operating in High–Gas Temperature Regimes: The Role of the Associative Ionization Reactions Involving Excited Atoms. *Plasma* **2020**, *3* (1), 12–26. https://doi.org/10.3390/plasma3010003.

(24) Klippenstein, S. J.; Harding, L. B.; Glarborg, P.; Miller, J. A. The Role of NNH in NO Formation and Control. *Combustion and Flame* **2011**, *158* (4), 774–789. https://doi.org/10.1016/j.combustflame.2010.12.013.

(25) Bozkaya, U.; Turney, J. M.; Yamaguchi, Y.; Schaefer, H. F., III. The Barrier Height, Unimolecular Rate Constant, and Lifetime for the Dissociation of HN2. *The Journal of Chemical Physics* **2010**, *132* (6), 064308. https://doi.org/10.1063/1.3310285.

(26) Hofmeister, A. M.; Whittington, A. G. Effects of Hydration, Annealing, and Melting on Heat Transport Properties of Fused Quartz and Fused Silica from Laser-Flash Analysis. *Journal of Non-Crystalline Solids* **2012**, *358* (8), 1072–1082. https://doi.org/10.1016/j.jnoncrysol.2012.02.012.